HHS Public Access

Author manuscript

Clin Nucl Med. Author manuscript; available in PMC 2018 October 01.

Published in final edited form as:

Clin Nucl Med. 2017 October ; 42(10): 735–740. doi:10.1097/RLU.0000000000001804.

^{18}F-DCFBC PSMA-Targeted PET/CT imaging in Localized Prostate Cancer: Correlation with mpMRI and Histopathology

Baris Turkbey, M.D.[*], **Esther Mena, M.D.**[*], **Liza Lindenberg, M.D.**, **Stephen Adler, Ph.D.**[⁂], **Sandra Bednarova, M.D.**, **Rose Berman, B.A.**, **Anita T. Ton, B.S.**, **Yolanda McKinney, R.N.**, **Philip Eclarinal, R.T.**, **Craig Hill, Ph.D.**, **George Afari, Ph.D.**, **Sibaprasad Bhattacharyya, Ph.D.**, **Ronnie C. Mease, Ph.D.**, **Maria J. Merino, M.D.**, **Paula M. Jacobs, Ph.D.**, **Bradford J. Wood, M.D.**, **Peter A. Pinto, M.D.**, **Martin Pomper, M.D, Ph.D.**, and **Peter L. Choyke, M.D.**

⁂Clinical Research Directorate/Clinical Monitoring Research Program, Leidos Biomedical Research, Inc., NCI Campus at Frederick, Frederick, Maryland 21702

Abstract

PURPOSE—To assess the ability of (N-[N-[(S)-1,3-dicarboxypropyl]carbamoyl]-4-^{18}F-fluorobenzyl-L-cysteine) (^{18}F-DCFBC), a prostate specific membrane antigen (PSMA) targeted positron emission tomography (PET) agent, to detect localized prostate cancer lesions in correlation with multi-parametric MRI (mpMRI) and histopathology.

METHODS—This HIPAA compliant, prospective IRB approved study included 13 evaluable patients with localized prostate cancer (median age=62.8 years [range 51–74], median PSA=37.5ng/dl [range 3.26–216]. Patients underwent mpMRI and ^{18}F-DCFBC PET/CT within a 3 months' window. Lesions seen on mpMRI were biopsied under TRUS/MRI fusion guidance or a radical prostatectomy was performed. ^{18}F-DCFBC PET/CT and mpMRI were evaluated blinded and separately for tumor detection on a lesion basis. For PET image analysis MRI and ^{18}F-DCFBC PET images were fused by using software registration and imaging findings were correlated with histology and uptake of ^{18}F-DCFBC in tumors was compared with uptake in benign prostatic hyperplasia (BPH) nodules and normal peripheral zone (PZ) tissue using the 80% threshold maximum standardized uptake value (SUV_{max}).

RESULTS—A total of 25 tumor foci (mean size=1.8cm; median size=1.5cm; range=0.6–4.7cm) were histopathologically identified in 13 patients. Sensitivity of ^{18}F-DCFBC PET/CT and mpMRI were 36% and 96%, respectively for all tumors. For index lesions, the largest tumor with highest Gleason score, sensitivity of ^{18}F-DCFBC PET/CT and mpMRI were 61.5% and 92%, respectively. The average SUV_{max} for primary prostate cancer was higher (5.8±4.4) than that of BPH nodules (2.1±0.3), or than normal prostate tissue (2.1±0.4), at 1 hour p.i. (p=0.0033).

CONCLUSION—The majority of index prostate cancers are detected with ^{18}F-DCFBC PET/CT and this may be a prognostic indicator based on uptake and staging. However, for detecting prostate cancer with high sensitivity, it is important to combine PSMA PET/CT with mpMRI.

Address Correspondence: Peter L. Choyke M.D., Director, Molecular Imaging Program, National Cancer Institute, Building 10, Room B3B69F, Bethesda, MD 20892, pchoyke@nih.gov, Phone: 301 402 8409, Fax: 301 402 3191.

[*]Drs. Turkbey and Mena equally contributed to this manuscript.

Keywords

Prostate cancer; ^{18}F-DCFBC PET/CT; Multi-parametric prostate MRI; PSMA

INTRODUCTION

Prostate cancer is the most common cancer type in men, and is the second leading cause of cancer related deaths in men in the United States (1). Until recently, diagnosis was based on an elevated prostate specific antigen (PSA) value and a random biopsy of the prostate. Multi-parametric MRI (mpMRI) has improved lesion detection in prostate cancer care by identifying suspicious lesions suitable for MRI-TRUS fusion biopsy. However, there is a considerable false positive rate for mpMRI and there is still no robust method to distinguish clinically significant cancers from indolent cancers other than biopsy. Moreover, local staging is relatively limited with mpMRI. A molecular imaging technique that could reliably identify intermediate and high risk cancers and stage them without detecting indolent cancers is needed.

Targeted imaging with positron emission tomography-computed tomography (PET/CT) has been extensively studied for more than a decade in order to address this and several tracers have been proposed such as ^{18}F-FDG, ^{11}C-Acetate, ^{18}F-Choline, ^{18}F-FACBC (fluciclovine) however, almost all of these tracers have been shown to have limited use in the setting of localized prostate cancer because they are taken up in benign conditions as well as malignancies and have a low sensitivity for extraprostatic disease. A major issue with these agents is a high false positive rate due to uptake in benign prostate hyperplasia (BPH) (2–4).

Prostate specific membrane antigen (PSMA) is a transmembrane protein that has been shown to be overexpressed in more aggressive prostate cancers (5). Recently, there has been growing interest in targeted imaging of PSMA using one of several PSMA-targeted agents which are labeled with ^{68}Ga (e.g. ^{68}Ga-PSMA-HBED-CC) or ^{18}F (e.g. ^{18}F-DCFBC and ^{18}F-DCFPyL) (6). Several research groups have reported improved prostate cancer detection in patients with biochemical recurrence and metastatic prostate cancer with radiolabeled PSMA targeted PET tracers. However, experience is still limited in PSMA PET imaging for localized primary prostate cancer (6,7).

The aim of our study was to assess the ability of (N-[N-[(S)-1,3-dicarboxypropyl]carbamoyl]-4-^{18}F-fluorobenzyl-L-cysteine) (^{18}F-DCFBC), a PSMA targeted PET agent, to detect localized prostate cancer lesions in correlation with mpMRI and histopathology.

METHODS

Study Design and Patient Population

This was a HIPAA compliant, prospective, single institution study, approved by the local institutional review board (IRB) with written informed consent, under an FDA approved IND (NCT02190279). Inclusion criteria included patients with histologically proven

prostatic adenocarcinoma. Exclusion criteria were contraindications to PET/CT scan or MRI, prior androgen deprivation therapy or histopathology that was not available.

Between July 2014–April 2016, 17 patients signed the consent form, and 16 of them (mean age 64 years, range: 51–74 years) underwent ^{18}F-DCFBC PET/CT imaging. One patient refused the tracer injection after signing the consent form and is excluded. All patients had mpMRI of the prostate at 3T within 3 months of the PET/CT imaging. Following imaging, all patients underwent either MRI/TRUS fusion guided biopsy or robotic assisted laparoscopic radical prostatectomy. Overall, there were 13 evaluable data sets for analysis; 3 patients were excluded from analysis, due to prior focal laser ablation therapy (n=1), prior brachytherapy (n=1), and lack of histopathology confirmation tissue (n=1).

^{18}F-DCFBC PET/CT Imaging and MRI Protocol

Details of ^{18}F-DCFBC PET/CT, ^{18}F-DCFBC preparation and MRI image acquisition protocols are presented in the supplement material.

Data Analysis

Histopathologic Analysis—All patients underwent MRI/TRUS fusion guided biopsy or robotic assisted laparoscopic radical prostatectomy and lymph node dissection. The prostatectomy specimens were fixed in formalin for 24–48-hours at room temperature. After fixation, the seminal vesicles were removed, and the gland was sliced, in axial orientation using a customized 3D printed mold, based on the preoperative MRI (8). Each slice was sequentially labeled and fixed for a further period of 24–48-hours, processed, and paraffin embedded as a whole mount. The tissue blocks were stained with hematoxylin-eosin. The resulting whole mount specimens were correlated with MRI and PET/CT imaging.

A pathologist (MJM with 30 years of experience) who was blinded to the imaging results independently reviewed the surgical specimens assessing for the presence of tumor, Gleason score, extracapsular extension and seminal vesicle invasion. For each patient, a dominant/index tumor (largest tumor with highest Gleason score) was determined.

Imaging Data and Histopathology Correlation—PET/CT images were registered and fused in the same plane as the MRI using commercial software (MIM 5.4 Software, MIM Software Inc. Cleveland, OH); the transmission CT was used to initially fuse the images with MRI using the pelvic bones as fiducial markers. As the PET and CT were already registered to each other, PET data was similarly brought into the MRI/CT “space”, resulting in the registration of the MRI and PET. Manual adjustments were necessary in all patients to accurately register the MRI and PET images to account for prostate motion and deformation.

Imaging Analysis

Visual Qualitative Analysis for Tumor Detection: One nuclear medicine physician (EM with experience of 6 years in PET/CT imaging), blinded to MRI and histopathology results, prospectively assessed the ^{18}F-DCFBC PET/CT scans. One radiologist (BT with 9 years of experience in prostate MRI), blinded to histopathology results, prospectively assessed the MRI scans. A lesion-based analysis was performed for each patient.

Lesion-based Analysis: On the 60 and 120 min post injection ^{18}F-DCFBC PET images, volumes of interest (VOIs) were created for each visually identified foci of ^{18}F-DCFBC uptake (greater than adjacent background), encompassing each entire visualized lesion. Time-activity curves were generated from the dynamic PET data (obtained in at the first 45 minutes). PET data was reconstructed into 25 frames using the following timing sequence; 4 time frames of 30 second duration, 8 time frames of 60 second duration, 10 time frames of 120 second duration and 3 time frames of 300 second duration. Contours were drawn on the registered MR scans delineating volumes containing tumor, BPH and normal tissue and transferred to the dynamic scan. The dynamic scan was spatially registered with the MR scan on which the contour regions of tumor, BPH and normal tissue were originally drawn. Additional contours were drawn on the iliac and bladder region directly on the dynamic scan, the former to obtain the input function for the pharmacokinetic modeling and the latter to evaluate the effects of the bladder activity on the prostate region over time. Time activity curve results of ^{18}F-DCFBC PET/CT is presented in supplement material.

For the MRI analysis, the reader, who was blinded to the PET results, used PIRADSv2 criteria to delineate focal lesions. (9).

Retrospective Quantitative Analysis: On fused PET/MRI true positive tumor foci, BPH nodules and normal prostate tissue were contoured in order to compare SUV_{max} within these three entities.

Staging Analysis: Clinical and pathologic TNM staging was done in each patient using American Joint Committee document (https://cancerstaging.org/references-tools/quickreferences/documents/prostatesmall.Pdf).

Statistical Analysis

For visual qualitative analysis, the sensitivities and positive predictive values of both mpMRI and ^{18}F-DCFBC PET/CT were calculated. SUV_{max} measurements of ^{18}F-DCFBC PET/CT imaging were obtained in tumor and non-tumor regions, including BPH and normal prostate tissue, and compared using a one-way analysis of variance (Anova). In addition, the ^{18}F-DCFBC SUV_{max} was correlated with tumor size, histopathologic Gleason score, and PSA values, using the Spearman rank correlation. The two-sample Wilcoxon test was used to compare SUV_{max} between those with a low Gleason score versus those with a high Gleason score (3+4 or lower vs 4+3 or higher, or between those with low PSA level and those with a high PSA level (≤10 ng/mL vs >10 ng/mL), results were presented as mean ± 1SD (p values < 0.05 were considered to represent a significant difference).

RESULTS

Clinical Findings

The evaluable study population consisted of 13 prostate cancer patients (mean age, 62.8 years; range, 51 to 74 years) who underwent TRUS/MRI fusion guided biopsy (n=9) or radical prostatectomy (n=4). ^{18}F-DCFBC injections were well-tolerated by all patients. At the time of ^{18}F-DCFBC PET scanning, the mean PSA level was 37.5 ng/mL

(median=16.53ng/ml), ranging from 3.26 ng/mL to 216 ng/mL. A total of 25 tumor foci, all >0.5 cm (mean size=1.8cm; median size=1.5cm; range=0.6–4.7cm) (n=4 Gleason 3+3, n=7 Gleason 3+4, n=6 Gleason 4+3, n=4 Gleason 4+4, n=4 Gleason 4+5) were histopathologically identified. Gleason scores of the tumors varied between 3+3 and 4+5. Considering all index tumors (largest tumor with highest Gleason score) per evaluable patient (n=13) (mean size=2.6cm; median=2cm; range=1.4–4.7cm) identified on pathology: four as 3+4, two as Gleason 4+3 (one of which has ductal adenocarcinoma features), three as 4+4, and four as 4+5 (Table 1). Four patients underwent radical prostatectomy with lymph node dissection, which revealed metastatic nodal involvement in 1 patient. Clinical and TNM staging of the patient cohort is presented in table 2.

Tumor Detection Rates of ^{18}F-DCFBC PET/CT and mpMRI

Lesion-Based Analysis—The lesion-based analysis for ^{18}F-DCFBC PET revealed 9 true positive (TP) tumor sites (mean size=2.6cm, median size=1.8 cm, range=1.4–4.7cm) [Figure 1, and Figure 2], 18 false negative (FN) sites (mean size=1.2cm, median size=1.3cm, range=0.6–2.1cm), with no false positive (FP) sites, which resulted in a sensitivity of 36% (9/25) but a positive predictive value (PPV) of 100% (9/9). For mpMRI, 24 sites were TP (mean size=1.8cm, median size=1.5cm, range=0.6–4.7cm), 1 FN (0.6cm in diameter) and 3 FP for tumor, resulting in a sensitivity of 96% (24/25) and a PPV of 89% (24/27). Sensitivity for index lesions were 92% (12/13) for mpMRI, and 61.5% (8/13) for ^{18}F-DCFBC PET, respectively.

Quantitative analysis—At 1 hour p.i., the average SUV_{max} of the histopathologically confirmed tumors (outlined on the MRI-registered to PET) was significantly higher (5.8±4.4, range 2.9–16.3) than that of normal prostate tissue (2.1±0.4; range 1.5–2.5), or than foci of benign prostatic hyperplasia (BPH) 2.1±0.3; range 1.5–2.5) (p=0.0033) (Figures 1, 2). Similarly, at 2 hours p.i. the average SUV_{max} of the histopathologically proven prostate tumors continued to be significantly higher (5.9±5.3, range 3.0–18.7) than normal prostate tissue (2.0±0.28; range 1.6–2.4) or than BPH foci (2.0±0.36; range 1.4–2.5) (p=0.012) (Figure 3). Moderate correlation was observed between SUV_{max} values and Gleason scores (r=0.6), however, there was no statistical significant difference between the SUV_{max} for tumors with lower Gleason score and higher Gleason scores (p=0.12) (Figure 4). No significant correlation was seen between SUV_{max} and PSA levels (r=0.30). Time activity curve results are presented in supplement section, however, dynamic evaluation of the data did not improve detection rates.

TNM Staging with ^{18}F-DCFBC PET/CT

Staging was performed pathologically in 4 patients and clinically in 9 patients. ^{18}F-DCFBC PET/CT staging was performed in 8 patients with positive agent uptake. Among the staged 8 patients, in 4 patients ^{18}F-DCFBC PET/CT under-staged tumor burden (n=2 tumor, n=1 nodal, n=1 both tumor and nodal). MRI performed correct T staging in 10/12 patients (n=1 patient could not be T staged at MRI since there was no visible lesion on MRI); for ^{18}F-DCFBC PET/CT T staging was available in 8 patients of whom 5 were correctly T staged. (table 2).

DISCUSSION

mpMRI with targeted prostate biopsy enables accurate detection of prostate cancer (10). However, currently available diagnostic techniques, including mpMRI, do not accurately assess prostate cancer aggressiveness or accurately perform local staging.. Accurate depiction of the location, stage and aggressiveness of index tumors may enable improved management of prostate cancer (11). PSMA targeting PET imaging is a promising new approach to accomplish this goal since PSMA expression is documented to correlate with prostate cancer aggressiveness (12). A recent study by Rowe et al. utilized ^{18}F-DCFBC PET/CT to accurately detect large volume Gleason 3+4 and higher grade prostate cancers in 13 patients. Moreover, they reported a moderate correlation between SUV and tumor Gleason grades as we also confirm in the current study (7). Moreover, PSMA targeted agents appear to differentiate benign prostate hyperplasia from prostate cancer with >2-fold higher uptake in the latter observed in this study. Similar findings have been reported by Fendler et al using ^{68}Ga-PSMA-HBED-CC PET/CT in 21 patients. They identified a significant SUV difference between prostate cancer and benign prostate tissue (11.8+/−7.6 vs. 4.9+/−2.9) with a similar >2-fold greater uptake in cancer (13). This is not true of other agents we have studied in a similar population with ^{11}C-Acetate and ^{18}F-FACBC PET imaging (3,4). Thus, PSMA PET/CT can differentiate cancer from BPH.

However, it is unclear whether PSMA PET/CT is superior to mpMRI for detecting clinically significant prostate cancer. In a study of 20 patients who underwent both mpMRI, ^{68}Ga-PSMA-HBED-CC the sensitivity, specificity, positive predictive value and negative predictive value for mpMRI and ^{68}Ga-PSMA-HBED-CC PET were approximately equal (for mpMRI: 44%, 94%, 81% and 76%, and for ^{68}Ga-PSMA-HBED-CC PET 49%, 95%, 85% and 88%, respectively). Based on these low sensitivity values in both imaging techniques, authors suggested potential complementarity of mpMRI and PSMA PET imaging (14). However, this is different from what we observed in the current study, where ^{18}F-DCFBC PET imaging detected only 61.5% of index lesions while mpMRI detected 95% of index lesions. The majority of the missed index lesions were Gleason 3+4 (4/6), but one was Gleason 4+4 and another was Gleason 4+3. mpMRI was much more sensitive especially for lesions <1cm in dimension compared to ^{18}F-DCFBC PET/CT imaging. While mpMRI was more sensitive in tumor detection, 18F-DCFBC PET exhibited a higher positive predictive value (100%). Thus, a positive 18F-DCFBC PET with a positive mpMRI is highly likely to yield a clinically significant index lesion. This may be useful in some patients in whom biopsy poses severe risks (e.g. prior sepsis requiring hospitalization or patients without a rectum).

Another potential utility of PSMA targeting PET imaging could be staging prostate cancer especially when they are high risk. Budaus et al. compared preoperative ^{68}Ga-PSMA PET/CT lymph node (LN) findings with surgical staging. Overall, 53 of 608 LNs had metastasis at histology in 12 of 30 patients (40%). ^{68}Ga-PSMA PET/CT identified 4 patients (33.3%) as LN true positive and 8 patients (66.7%) as false negative. Overall sensitivity, specificity, positive predictive value, and negative predictive value of ^{68}Ga-PSMA PET/CT for LN metastasis detection were 33.3%, 100%, 100%, and 69.2%, respectively (15). In our cohort, we compared the overall TNM staging of ^{18}F-DCFBC PET/CT with clinical and

pathological (whenever available) staging. Among eight patients in whom a true positive tumor was detected by ^{18}F-DCFBC PET/CT imaging, TNM staging showed concordance with clinical or pathological staging in 4 patients; whereas in the other 4 patients, ^{18}F-DCFBC PET/CT imaging under-staged including one false negative node, one false negative T3a and N1 staging, one false negative seminal vesicle invasion and one false negative T2c staging due to a missed intraprostatic lesion in the contralateral lobe. Although the staging results were limited in number, these preliminary findings are consistent with a relatively low accuracy for staging compared to surgery. This is likely due to the small volume of such nodal metastases but this finding should be explored in more detail before PSMA PET/CT is introduced as a staging tool. It is also possible that 2nd generation agents such as ^{18}F-DCFPyl may perform better as there is both higher affinity and decreased background with these agents (16,17).

Our study has several limitations; first, our study included only a limited number of patients and tumors. Second, we fused PET and MRI and histopathology data using a semi-automated mutual information technique followed by minor manual adjustments. This approach does not account for prostate deformation due to the endorectal coil or from the deformation due to pathology fixation of the specimen which could cause some misregistration. We do not believe this caused a problem in the analysis since we were always able to match lesions visually. Finally, ^{18}F-DCFBC demonstrated a moderate amount of background blood pool activity which was also reported by Rowe et al. and potentially limits the sensitivity of this agent in soft tissues by decreasing the tumor-to-background ratio, which can ultimately limit detection of cancer (7). The second generation compound of ^{18}F-labeled PSMA is ^{18}F-DCFPyL, which has been reported to have less background blood pool activity and more tumor specific uptake (18) is likely to perform better. We will shortly begin testing this agent in a clinical trial.

CONCLUSION

^{18}F-DCFBC PET/CT has lower sensitivity than mpMRI in detecting prostate cancer but has a higher positive predictive value, suggesting a potential role in patients at high risk for biopsy. It clearly identifies cancers in comparison to BPH. There is a moderate correlation of uptake and Gleason grade. Dynamically acquired PET data does not add sensitivity or specificity to the examination. Limited data suggests that PSMA PET tends to understage prostate cancer. The second generation of this agent, ^{18}F-DCFpyl may reduce some of these limitations.

Supplementary Material

Refer to Web version on PubMed Central for supplementary material.

Acknowledgments

This research was funded in part by Cancer Imaging program, National Institutes of Health, National Cancer Institute. We acknowledge the NExT program of NCI for supporting this research. This project has been funded in whole or in part with federal funds from the National Cancer Institute, National Institutes of Health, under Contract No. HHSN261200800001E. The content of this publication does not necessarily reflect the views or policies of the

Department of Health and Human Services, nor does mention of trade names, commercial products, or organizations imply endorsement by the U.S. Government.

Abbreviations

PET/CT	positron emission tomography computed tomography
PSA	prostate specific antigen
mpMRI	multi-parametric magnetic resonance imaging
TRUS	transrectal ultrasonography
FDG	fluorodeoxyglucose
FACBC	fluciclovine
BPH	benign prostatic hyperplasia
PSMA	prostate specific membrane antigen
SUVmax	maximum standardized uptake value
TNM	tumor, node, metastases
TP	true positive
FP	false positive
FN	false negative
PPV	positive predictive value

References

1. Siegel RL, Miller KD, Jemal A. Cancer statistics, 2016. CA Cancer J Clin. 2016; 66:7–30. [PubMed: 26742998]
2. Liu IJ, Zafar MB, Lai YH, Segall GM, Terris MK. Fluorodeoxyglucose positron emission tomography studies in diagnosis and staging of clinically organ-confined prostate cancer. Urology. 2001; 57:108–111. [PubMed: 11164153]
3. Mena E, Turkbey B, Mani H, et al. 11C-Acetate PET/CT in localized prostate cancer: a study with MRI and histopathologic correlation. J Nucl Med. 2012; 53:538–545. [PubMed: 22343504]
4. Turkbey B, Mena E, Shih J, et al. Localized prostate cancer detection with 18F FACBC PET/CT: comparison with MR imaging and histopathologic analysis. Radiology. 2014; 270:849–856. [PubMed: 24475804]
5. Bostwick DG, Pacelli A, Blute M, Roche P, Murphy GP. Prostate specific membrane antigen expression in prostatic intraepithelial neoplasia and adenocarcinoma: a study of 184 cases. Cancer. 1998; 82:2256–2261. [PubMed: 9610707]
6. Rowe SP, Gorin MA, Allaf ME, et al. PET imaging of prostate-specific membrane antigen in prostate cancer: current state of the art and future challenges. Prostate Cancer Prostatic Dis. 2016; 19:223–230. [PubMed: 27136743]
7. Rowe SP, Gage KL, Faraj SF, et al. (1)(8)F-DCFBC PET/CT for PSMA-Based Detection and Characterization of Primary Prostate Cancer. J Nucl Med. 2015; 56:1003–1010. [PubMed: 26069305]

8. Shah V, Pohida T, Turkbey B, et al. A method for correlating in vivo prostate magnetic resonance imaging and histopathology using individualized magnetic resonance-based molds. Rev Sci Instrum. 2009; 80:104301. [PubMed: 19895076]

9. Barentsz JO, Weinreb JC, Verma S, et al. Synopsis of the PI-RADS v2 Guidelines for Multiparametric Prostate Magnetic Resonance Imaging and Recommendations for Use. Eur Urol. 2016; 69:41–49. [PubMed: 26361169]

10. Siddiqui MM, Rais-Bahrami S, Turkbey B, et al. Comparison of MR/ultrasound fusion-guided biopsy with ultrasound-guided biopsy for the diagnosis of prostate cancer. Jama. 2015; 313:390–397. [PubMed: 25626035]

11. Stamey TA, McNeal JE, Yemoto CM, Sigal BM, Johnstone IM. Biological determinants of cancer progression in men with prostate cancer. Jama. 1999; 281:1395–1400. [PubMed: 10217055]

12. Osborne JR, Green DA, Spratt DE, et al. A prospective pilot study of (89)Zr-J591/prostate specific membrane antigen positron emission tomography in men with localized prostate cancer undergoing radical prostatectomy. J Urol. 2014; 191:1439–1445. [PubMed: 24135437]

13. Fendler WP, Schmidt DF, Wenter V, et al. 68Ga-PSMA-HBED-CC PET/CT detects location and extent of primary prostate cancer. J Nucl Med. 2016

14. Rhee H, Thomas P, Shepherd B, et al. Prostate Specific Membrane Antigen Positron Emission Tomography May Improve the Diagnostic Accuracy of Multiparametric Magnetic Resonance Imaging in Localized Prostate Cancer. J Urol. 2016

15. Budaus L, Leyh-Bannurah SR, Salomon G, et al. Initial Experience of (68)Ga-PSMA PET/CT Imaging in High-risk Prostate Cancer Patients Prior to Radical Prostatectomy. Eur Urol. 2016; 69:393–396. [PubMed: 26116958]

16. Dietlein M, Kobe C, Kuhnert G, et al. Comparison of [(18)F]DCFPyL and [(68)Ga]Ga-PSMA-HBED-CC for PSMA-PET Imaging in Patients with Relapsed Prostate Cancer. Mol Imaging Biol. 2015; 17:575–584. [PubMed: 26013479]

17. Dietlein F, Kobe C, Neubauer S, et al. PSA-stratified performance of 18F- and 68Ga-labeled tracers in PSMA-PET imaging of patients with biochemical recurrence of prostate cancer. J Nucl Med. 2016

18. Szabo Z, Mena E, Rowe SP, et al. Initial Evaluation of [(18)F]DCFPyL for Prostate-Specific Membrane Antigen (PSMA)-Targeted PET Imaging of Prostate Cancer. Mol Imaging Biol. 2015; 17:565–574. [PubMed: 25896814]

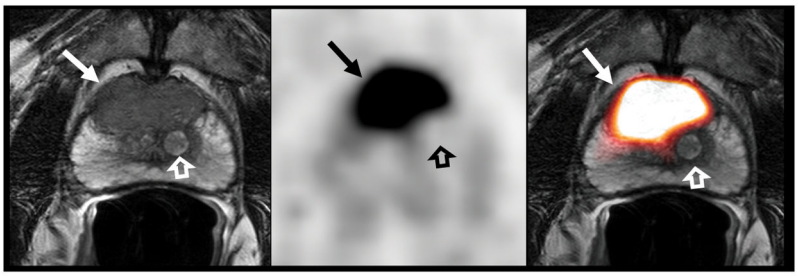

Figure 1.

73-year-old man with a serum PSA level of 38.6 ng/mL. T2W MR image (A), axial ^{18}F-DCFBC PET image (B) and fused MRI/PET image (C) demonstrate a large low-signal-intensity focus in the anterior mid-central gland (arrow), which shows intense ^{18}F-DCFBC uptake with SUV_{max} up to 16.3. Histopathology confirmed a Gleason score 4+5 prostate cancer. The BPH nodule (open arrow) and the normal prostate tissue does not demonstrate abnormal DCFBC uptake.

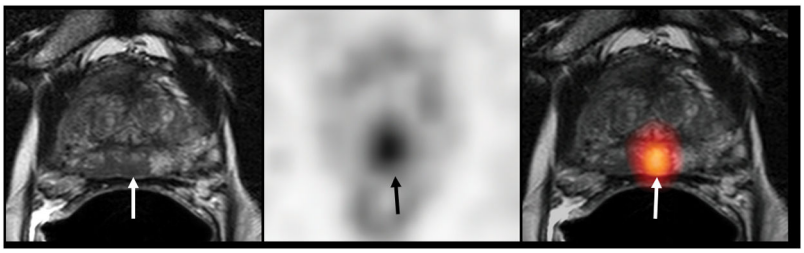

Figure 2.

54-year-old man with serum PSA levels of 10.8 ng/mL. T2W MR image (A), axial ^{18}F-DCFBC PET image (B) and fused MR/PET image (C) demonstrate a 1.5 cm low-signal-intensity focus in the apical-mid peripheral zone lesion (arrow), which shows focal intense ^{18}F-DCFBC uptake, with SUV_{max} up to 4.2. Biopsy confirmed a Gleason 4+4 primary prostate cancer.

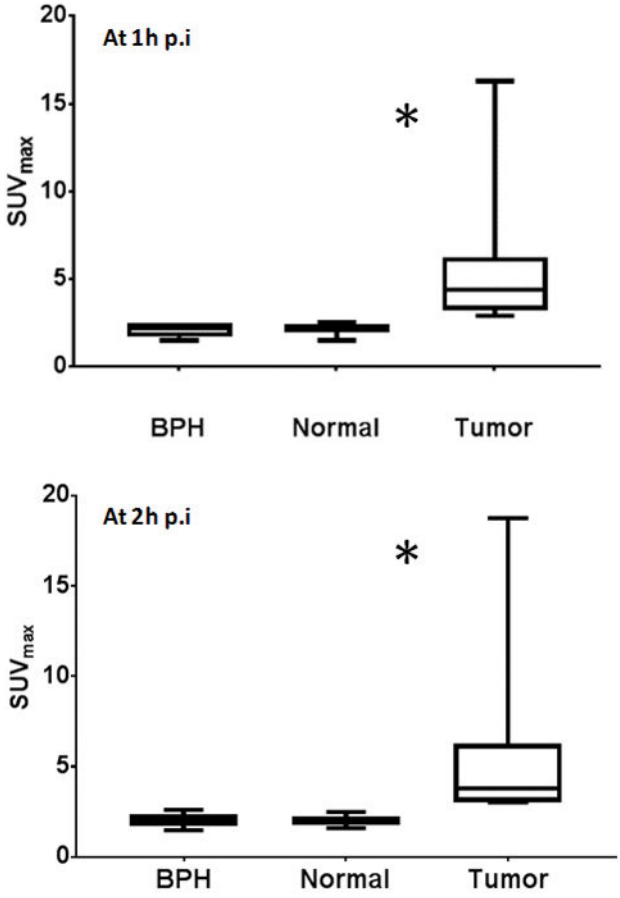

Figure 3.

Pathologically confirmed prostate tumors (outlined on the MRI-registered to PET) showed significant higher ^{18}F-DCFBC uptake than benign prostatic hyperplasia (BPH) or normal prostate areas, at 1 hour (p=0.0033) and at 2 hours (p=0.012). p.i.

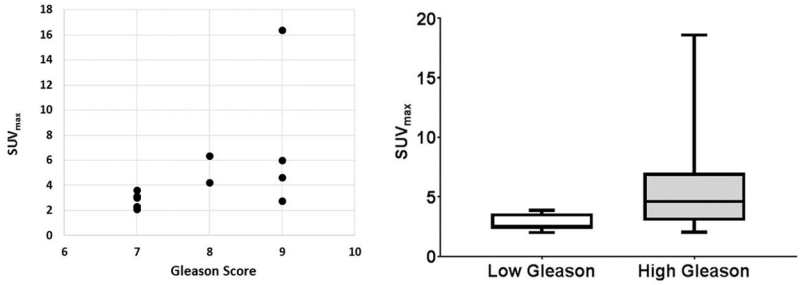

Figure 4.

Scatterplot of 18F-DCFBC PET SUVmax and prostate lesions' Gleason score demonstrating moderate positive correlation (r=0.6). However, there was no statistical significant difference between the SUVmax for tumors with lower Gleason score and higher Gleason scores (p=0.12).

Table 1

Index Lesion ^{18}F-DCFBC PET Characteristics.

Patient	Age	Serum PSA (ng/ml)	Index lesion	18F-DCFBC visual analysis (lesion visibility)	SUV_{max} at 1hr p.i.
1	73	38.64	Gleason 4+5	positive	16.3
2	67	46.47	Gleason 4+5	positive	4.6
3	51	4.36	Gleason 4+3	positive	3.1
4	53	49.92	Gleason 4+5	positive	5.9
5	59	9.61	Gleason 3+4	negative	2.1
6	66	216.4	Gleason 4+4	positive	6.3
7	69	47.03	Gleason 4+5	positive	2.7
8	55	16.53	Gleason 3+4	negative	2.3
9	66	8.71	Gleason 3+4	positive	3.6
10	72	26.02	Gleason 4+4	negative	2.3
11	74	3.24	Gleason 3+4	equivocal	3.0
12	53	3.26	Gleason 4+3 (with ductal features)	equivocal	3.1
13	54	10.85	Gleason 4+4	positive	4.2

Table 2

^{18}F-DCFBC, pathological/clinical and MRI staging results.

Patient	Age	Serum PSA (ng/ml)	Index lesion	MRI staging	18F-DCFBC Staging	Pathologic/clinical staging
1	73	38.64	Gleason 4+5	T3a,Nx,Mx	T3a,N0,M0	T3a,N0,M0
2	67	46.47	Gleason 4+5	T3b,Nx,Mx	T3b,N0,M0	T3b,N1,M0
3	51	4.36	Gleason 4+3	T2a,Nx,Mx	T2a,N0,M0	pT2,pN0,M0
4	53	49.92	Gleason 4+5	T3b,Nx,Mx	T2c,N0,M0	T3b,N0,M0
5	59	9.61	Gleason 3+4	T2b,Nx,Mx	NA	pT3a,pN0,M0
6	66	216.4	Gleason 4+4	T3b,Nx,Mx	T3b,N1,M0	T3b,N1,M0
7	69	47.03	Gleason 4+5	T2c,Nx,Mx	T2a,N0,M0	pT3a,N1,M0
8	55	16.53	Gleason 3+4	T3a,Nx,Mx	NA	T3a,N0,M0
9	66	8.71	Gleason 3+4	T2c,Nx,Mx	T2c,N0,M0	T2c,N0,M0
10	72	26.02	Gleason 4+4	T3a,Nx,Mx	NA	T3a,N0,M0
11	74	3.24	Gleason 3+4	T3a,Nx,Mx	NA	T3a,N0,M0
12	53	3.26	Gleason 4+3 (with ductal features)	NA	NA	pT2,pN0,M0
13	54	10.85	Gleason 4+4	T2c,Nx,Mx	T2a,N0,M0	T2c,N0,M0